℘

Discovery of Localized Regions of Excess 10-TeV Cosmic Rays

A. A. Abdo,[1] B. Allen,[2] T. Aune,[3] D. Berley,[4] E. Blaufuss,[4] S. Casanova,[5] C. Chen,[6] B. L. Dingus,[7] R. W. Ellsworth,[8]
L. Fleysher,[9] R. Fleysher,[9] M. M. Gonzalez,[10] J. A. Goodman,[4] C. M. Hoffman,[7] P. H. Hüntemeyer,[7] B. E. Kolterman,[9]
C. P. Lansdell,[11] J. T. Linnemann,[12] J. E. McEnery,[13] A. I. Mincer,[9] P. Nemethy,[9] D. Noyes,[4] J. Pretz,[7] J. M. Ryan,[14]
P. M. Saz Parkinson,[3] A. Shoup,[15] G. Sinnis,[7] A. J. Smith,[4] G. W. Sullivan,[4] V. Vasileiou,[4] G. P. Walker,[16]
D. A. Williams,[3] and G. B. Yodh[6]

(Milagro Collaboration)

[1]*Naval Research Laboratory, Washington, D.C., USA*
[2]*Harvard-Smithsonian Center for Astrophysics, Cambridge, Massachusetts, USA*
[3]*University of California, Santa Cruz, California, USA*
[4]*University of Maryland, College Park, Maryland, USA*
[5]*Max Planck Institut für Kernphysik, Heidelberg, Germany*
[6]*University of California, Irvine, California, USA*
[7]*Los Alamos National Laboratory, Los Alamos, New Mexico, USA*
[8]*George Mason University, Fairfax, Virginia, USA*
[9]*New York University, New York, New York, USA*
[10]*Instituto de Astronomia, Universidad Nacional Autonoma de Mexico, D.F., Mexico*
[11]*Institute for Defense Analyses, Alexandria, Virginia, USA*
[12]*Michigan State University, East Lansing, Michigan, USA*
[13]*NASA Goddard Space Flight Center, Greenbelt, Maryland, USA*
[14]*University of New Hampshire, Durham, New Hampshire, USA*
[15]*Ohio State University, Lima, Ohio, USA*
[16]*National Security Technologies, Las Vegas, Nevada, USA*

The 7 year data set of the Milagro TeV observatory contains 2.2×10^{11} events of which most are due to hadronic cosmic rays. These data are searched for evidence of intermediate scale structure. Excess emission on angular scales of $\sim 10°$ has been found in two localized regions of unknown origin with greater than 12σ significance. Both regions are inconsistent with pure gamma-ray emission with high confidence. One of the regions has a different energy spectrum than the isotropic cosmic-ray flux at a level of 4.6σ, and it is consistent with hard spectrum protons with an exponential cutoff, with the most significant excess at ~ 10 TeV. Potential causes of these excesses are explored, but no compelling explanations are found.

The flux of charged cosmic rays at TeV energies is known to be nearly isotropic. This is due to Galactic magnetic fields, which randomize the directions of charged particles. However, numerous experiments across a wide range of energies have found anisotropy on large angular scales, typically with a fractional amplitude of $\sim 10^{-3}$ (see [1–5], for example). Large-scale anisotropy is also seen in data from the Milagro detector [6]; here we present the results of an analysis sensitive to intermediate angular scales ($\sim 10°$).

Milagro [7] is a water Cherenkov air shower detector located in New Mexico, USA at an altitude of 2630 m and at 36° N latitude. It is composed of a central 60 m $\times$ 80 m pond surrounded by a sparse 200 m $\times$ 200 m array of 175 "outrigger" water tanks. The pond is instrumented with 723 photomultiplier tubes (PMTs) in two layers. The top layer and outrigger tanks are used to determine the direction and energy, while the bottom layer is used to distin-guish between gamma-ray induced and hadron induced air showers. The outriggers, with each tank containing a single PMT, improve the angular and energy resolution of the detector for events collected after May, 2003. Milagro has a ~ 2 sr field of view, operates with a $>90\%$ duty cycle, and has a trigger rate from cosmic rays of ~ 1700 Hz, making it well suited to searching for anisotropy in the arrival directions of TeV cosmic rays.

For studies on small to intermediate scales ($\leq 10°$), an adaptation of the gamma-ray point source analysis, which has been published previously [7], is used. The primary difference between the previous analysis and the current analysis is that no cosmic-ray background rejection cuts are made. These cuts removed over 90% of the events, so the analysis reported here uses nearly 10 times the number of events of the previous analysis. Like the previous analysis, a signal map is made based on the arrival direction of each event. A background map is also created using the

"direct integration" technique [7], in which two-hour intervals are used to calculate the background. Because of this two-hour interval, the analysis is relatively insensitive to features larger than $\sim 30°$ in right ascension (RA); a different analysis of the Milagro data sensitive to larger features has been performed and is presented elsewhere [6].

In the gamma-ray point source analysis, the signal and background maps are smoothed with a square bin of size $2.1°/\cos(\delta)$ in RA by $2.1°$ in declination (δ), which is optimal for Milagro's angular resolution. However, the bin size may be increased to improve the sensitivity to larger features, with a maximum size of about $10°$ for $\delta < 60°$ (for $\delta > 60°$, the RA bin width $10°/\cos(\delta)$ becomes too large for the $30°$ background interval). The significance is calculated using the method of Li and Ma [8].

The analysis has been applied to data collected between July 2000 and August 2007. Events were required to have a zenith angle $<45°$ and nFit ≥ 20, where nFit is the number of PMTs used in the angle fit. With these cuts, the data set consists of 2.2×10^{11} events with a median energy of ~ 1 TeV and an average angular resolution of $<1°$. Figure 1 shows the map of significances made with $10°$ smoothing and no cuts to discriminate gamma rays from charged cosmic rays. The Cygnus region, which has previously been shown to emit TeV gamma rays [9], is clearly visible. The excesses labeled "region A" and "region B" are seen with peak significances of 15.0σ and 12.7σ, respectively. These are pretrial significances because the location and extent of the excesses were determined by examining the data. A map such as shown in Fig. 1 has a few 100 000 independent bins, but given the high statistical significance many maps could be examined and the posttrial's significance would be reduced by $<1\sigma$. The fractional excess relative to the cosmic-ray background is $\sim 6 \times 10^{-4}$ for region A and $\sim 4 \times 10^{-4}$ for region B. Note that both excesses are paralleled by regions of deep

deficit; this is a known effect of the analysis due to the fact that regions A and B are included in the background calculation of neighboring areas in RA. Therefore, the excess raises the background calculation above its actual value, resulting in an apparent deficit.

Similarity is seen between the map in Fig. 1 and results from the Tibet AS γ collaboration [3,10], but a direct comparison cannot be made because the analysis methods differ. For each band in δ, the Tibet analysis measured the excess (or deficit) relative to the average for that δ band, making it sensitive to the large-scale anisotropy discussed in [3]. Smaller features, such as regions A and B, were superimposed on the large-scale variation, which is several times greater in amplitude. Conversely, in the analysis presented here, the excess or deficit was measured with respect to the local background calculation, which is determined from the data $\pm 30°$ in RA. This is illustrated in Fig. 2, which shows the data and background calculation versus RA for a $10°$ band in declination without any smoothing applied to the data. The large-scale variation dominates the figure, but the background calculation makes the analysis sensitive only to features with an extent smaller than $\sim 30°$ in RA. It is noteworthy that the Tibet AS γ collaboration has developed a model for the large-scale structure, and the residual map after subtracting that model from their data shows excesses similar to regions A and B [10].

To estimate the extent of region A, an elliptical Gaussian was fit to the excess map of the data in $0.1°$ bins prior to smoothing. The fit, which accounted for the change in sensitivity with declination, returned a centroid of RA = $69.4° \pm 0.7°$, $\delta = 13.8° \pm 0.7°$, a half width of $2.6° \pm 0.3°$, a half length of $7.6° \pm 1.1°$, and an angle of $46° \pm 4°$ with respect to the RA axis. It is important to note that this fit focused on a "hot spot" in the general excess of region A, but there is still excess extending to lower
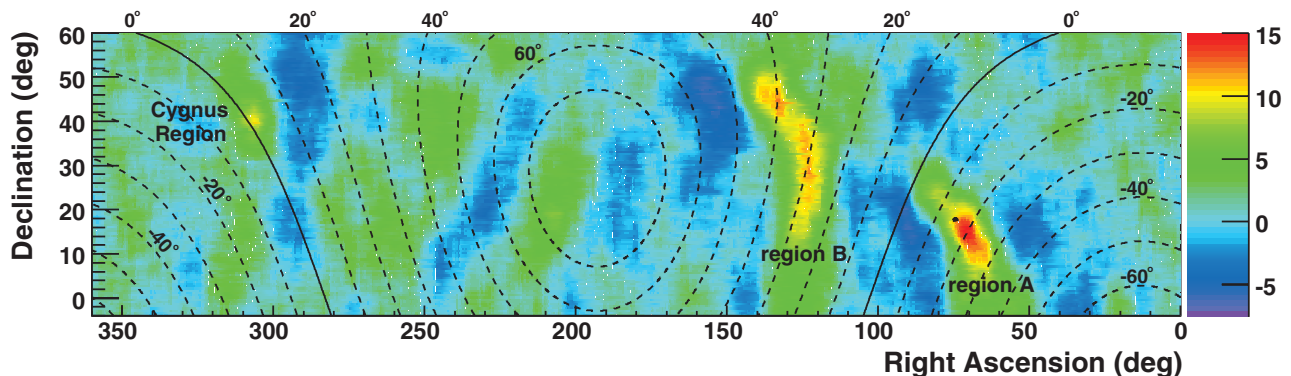

FIG. 1 (color).   Map of significances for the Milagro data set without any cuts to remove the hadronic cosmic-ray background. A $10°$ bin was used to smooth the data, and the color scale gives the significance. The solid line marks the Galactic plane, and every $10°$ in Galactic latitude are shown by the dashed lines. The black dot marks the direction of the heliotail, which is the direction opposite the motion of the solar system with respect to the local interstellar matter. The fractional excess of region A is $\sim 6 \times 10^{-4}$, while for region B it is $\sim 4 \times 10^{-4}$. The deep deficits bordering the regions of excess appear because the background calculation has been raised by the excess.
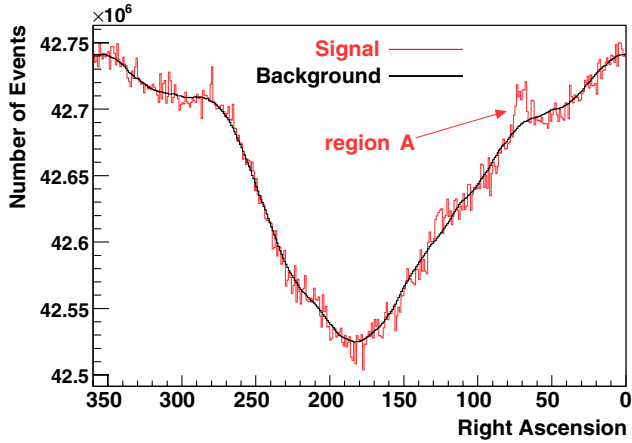
FIG. 2 (color online).   Signal and background events vs RA for
$10° < \delta < 20°$. The plot was made using independent $10°$ δ by
$1°$ RA bins (i.e., no smoothing). A subset of the data was used in
which there are only full days of data in order to give an
approximately uniform exposure in RA. Region A corresponds
to the excess at RA $\approx 70°$. This plot shows that the region A
excess is inherent in the raw signal data and is not due to an
underestimation of the background.

declinations. A fit was not performed to the excess in
region B due to its large, irregular shape.

While the excesses in regions A and B are statistically
significant, systematic causes must be ruled out. Potential
weather-related effects were explored by dividing the data
into the four seasons, and both excesses were seen in each
season. The data were also divided into yearly data sets to
investigate whether changes to the detector could play a
role, and again the excesses were found in each data set.
The analysis was also run using universal time instead of
sidereal time to check for day-night effects which could
masquerade as a signal. In addition, the data were analyzed
using antisidereal time, which provides a sanity check on
the analysis since it will scramble real celestial features.
No excess appears in either analysis.

Potential errors in the background calculation were also
investigated. Figure 2 shows the number of events versus
RA for the signal and background for $10° < \delta < 20°$,
using independent $10° \delta$ by $1°$ RA bins (i.e., no smooth-
ing). The data for this figure were chosen to include only
full days in order to achieve an approximately uniform
exposure as a function of RA, and the broad deficit seen by
the Tibet Air Shower Array is evident (centered around
RA $= 180°$). As can be seen, the background estimate as
calculated via the direct integration technique [7] agrees
well with the data. The excess corresponding to region A is
clearly inherent in the raw signal data and is not an artifact
created by the background subtraction. A similar result is
found for region B.

Diagnostic tests have been performed to gain insight into
the nature of regions A and B. For the purposes of these
tests, region A is defined as the box bounded by $66° <$

RA $< 76°$ and $10° < \delta < 20°$. Region B is defined as the
union of two boxes: $117° <$ RA $< 131°$ and $15° < \delta <
40°$, and $131° <$ RA $< 141°$ and $40° < \delta < 50°$. These
definitions were chosen by visual inspection of Fig. 1.

To check for flux variation, the analysis was applied to
yearly and seasonal data sets. For each region, the yearly
excess was consistent with a constant flux. Both regions
also had a significant excess during each of the four sea-
sons, with the respective fractional excess in parts per
10 000 in spring, summer, fall, and winter of 6.5 ± 0.9,
4.0 ± 0.9, 6.4 ± 0.9, 7.2 ± 0.9 for region A and 3.5 ± 0.4,
3.3 ± 0.4, 4.0 ± 0.4, 4.7 ± 0.4 for region B. In both cases
the fractional excess was lowest in the summer and highest
in the winter, and the χ^2 probability relative to a constant
fractional excess is only about 5% for each region. While
this may provide insight into the cause of these excesses,
only statistical errors are given. There could be systematic
effects such as the slightly higher energy threshold of
Milagro in winter when there is snow on top of the pond.

The excesses in regions A and B are inconsistent with
pure gamma-ray emission. We can statistically separate
gamma-ray events from cosmic-ray events utilizing two
parameters. The compactness parameter [7] uses PMT
information in the bottom layer of Milagro to identify the
penetrating particles characteristic of a hadronic air
shower. The distribution of compactness depends on the
energy spectrum of the source with higher energy gamma
rays producing showers of greater compactness. In order to
exclude a gamma-ray hypothesis of any spectrum, we also
fit an energy parameter f_{out}, the fraction of outrigger PMTs
that detect light. Figure 3(a) shows the fractional excess of
$\log_e(f_{out})$ for regions A and B. We hypothesize a spectrum
for the excess of the form

$$dN/dE \propto E^\gamma e^{-(E/E_c)}, \qquad (1)$$

where γ is the spectral index and E_c is the characteristic
energy at which the spectrum cuts off. We attempt this fit
for regions A and B assuming separately that the primary
particles are purely gamma rays and purely protons. The
gamma-ray hypothesis in region A has a χ^2 of 124.0 with
16 degrees of freedom. The cosmic-ray hypothesis pro-
duces a reasonable fit, with a minimum χ^2 of 10.3. For
region B, the best gamma-ray hypothesis has a χ^2 of 84.8
compared to a best cosmic-ray hypothesis of $\chi^2 = 19.0$,
again with 16 degrees of freedom. Thus the proton hy-
pothesis is a reasonable fit for both regions and the gamma-
ray hypothesis is inconsistent with probabilities of $9 \times
10^{-19}$ for region A and 2×10^{-11} for region B. The pos-
sibility that the regions contain some admixture of protons
and gamma rays has not been considered. Figure 4 shows
the 1σ, 2σ, and 3σ regions around the best fit for region A
and region B for the pure-proton hypothesis. Some care
must be taken in interpreting Fig. 4. It does not account for
our systematic errors. There is a estimated systematic
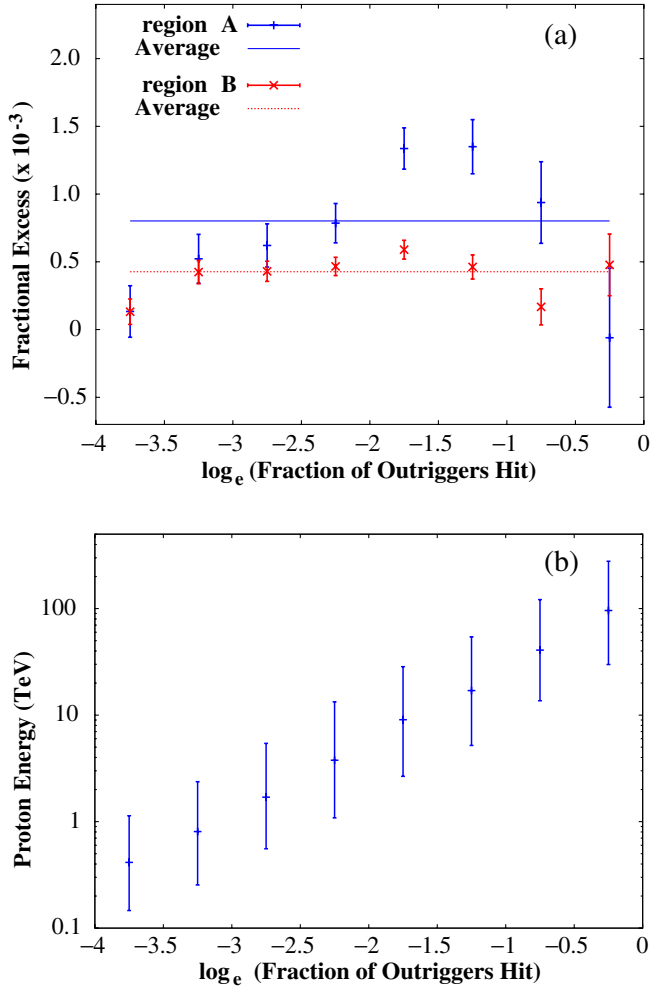uncertainty in the spectral index of ±0.2 due to variation

FIG. 3 (color online). (a) Differential plot of the fractional
excess versus $\log_e(f_{out})$ for regions A and B, where f_{out} is the
fraction of the outriggers hit. The spectrum of region A is
significantly different than the background (2×10^{-6}), which
is represented by the horizontal line. (b) Profile plot of the
simulated energy of protons for the as a function of $\log_e(f_{out})$.
The ranges are asymmetric and contain the inner 68% of
simulated events.

in the trigger threshold (caused by such things as changes
in atmospheric pressure or ice on the pond). There is also a
~30% systematic uncertainty in the energy scale due to the
threshold variation, as well as discrepancy between the
simulated and measured trigger rates. The fit does not
constrain the spectrum well except to suggest that a hard
spectrum is favored, particularly for region A. The cutoff
energy is constrained, with $\log_{10}(E_c/\text{GeV}) = 4.0^{+0.4}_{-0.5(\text{stat})}$
for region A and $\log_{10}(E_c/\text{GeV}) = 4.0^{+0.3}_{-0.5(\text{stat})}$ for region
B. Most importantly, the pure gamma-ray hypothesis is
strongly disfavored.

We can see that the excesses in regions A and B are
harder than the spectrum of the isotropic part of cosmic
rays with minimal systematic effects by looking at the data
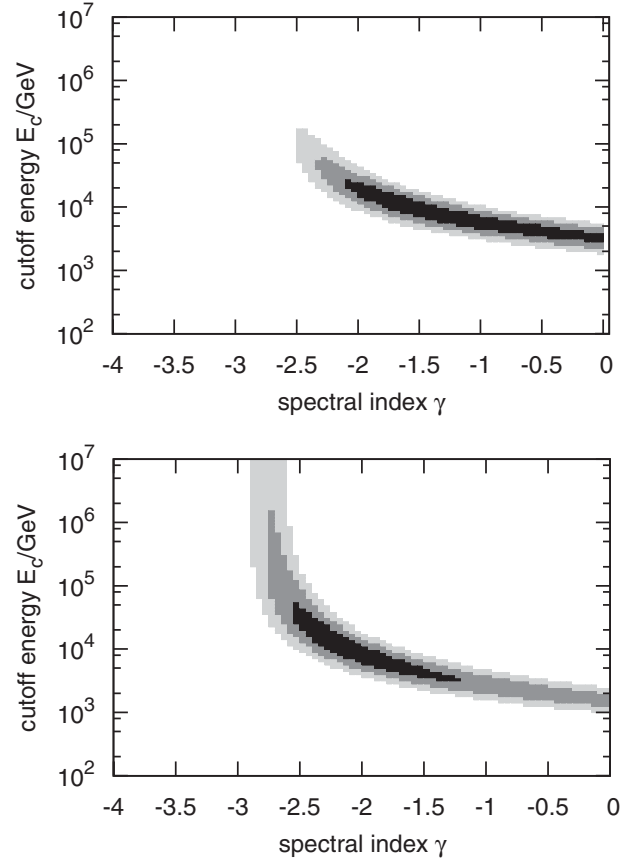alone. Figure 3(a) shows the fractional excess in regions A

FIG. 4. Results of a χ^2 fit to the excesses in regions A and B,
assuming a pure-proton spectrum of the form in Eq. (1). The top
panel shows the results for region A and the bottom panel shows
the results for region B. The 1σ, 2σ and 3σ allowed regions of
the spectral index γ and the cutoff energy E_c are indicated by the
shaded regions.

and B as a function of f_{out}. Assuming that the excess is due
to cosmic rays of the same spectrum, we would expect the
fractional excess to be completely flat. The offset from zero
tells us that this region is in fact an excess. A χ^2 test of
whether the curves in Fig. 3 are flat for region $A(B)$ returns
a chance probability of 2×10^{-6} (6×10^{-3}), independent
of systematic errors. The excess of region A is most sig-
nificantly detected for $\log_e(f_{out}) \sim -1.5$, corresponding
to an energy of about 10 TeV for protons, as shown in
Fig. 3(b). At around 10 TeV, the spectrum cuts off consis-
tent with the results of the spectral fit.

There is currently no compelling explanation for the
excesses in regions A and B. One possibility is that they
could be due to neutrons, but this is unlikely because the
decay length of 10 TeV neutrons is only about 0.1 parsecs,
which is much closer than the nearest star. Another possi-
bility is that these excesses could be caused by a Galactic
cosmic-ray accelerator, but this is difficult because the
gyroradius of a 10 TeV proton in a 2 μG magnetic field,
which is the estimated strength of the local Galactic field
[11], is only ~0.005 parsecs. In order for protons from a

cosmic-ray accelerator to reach us, the intervening magnetic field must connect us to the source and be coherent out to ~100 parsecs since there are likely no sources within this distance. However, the direction of both regions is nearly perpendicular to the expected Galactic magnetic field direction [11] With nonstandard cosmic-ray diffusion, it is conceivable to account for these regions with a nearby cosmic-ray accelerator [12].

Another possibility is that one or both of the excesses could be caused by the heliosphere. This explanation is supported by the coincidence of region A with the direction of the heliotail (RA $\approx 74°$, $\delta \approx 17°$ [13]), which is the direction opposite the motion of the solar system with respect to the local interstellar matter. The possibility that we are seeing neutron production in the gravitationally-focused tail of interstellar medium material has been considered and discarded in [12] because of insufficient target material.

In summary, Milagro has observed two unexplained regions of excess with high significance. Potential systematic causes have been examined and excluded. Both excesses are inconsistent with pure gamma rays with high confidence, and their energy spectra are moderately to strongly inconsistent with the spectrum of the isotropic cosmic-ray flux. In particular, the excess in region A can be modeled as hard spectrum protons with a cutoff.

[1] K. Nagashima, K. Fujimoto, and R. M. Jacklyn, J. Geophys. Res. **103**, 17 429 (1998).
[2] D. L. Hall *et al.*, J. Geophys. Res. **104**, 6737 (1999).
[3] M. Amenomori *et al.*, Science **314**, 439 (2006).
[4] M. Ambrosio *et al.*, Phys. Rev. D **67**, 042002 (2003).
[5] K. Munakata *et al.*, Phys. Rev. D **56**, 23 (1997).
[6] B. E. Kolterman *et al.*, 30th ICRC, Merida, Mexico (2007).
[7] R. Atkins *et al.* (Milagro Collaboration), Astrophys. J. **595**, 803 (2003).
[8] T. P. Li and Y. Q. Ma, Astrophys. J. **272**, 317 (1983).
[9] A. A. Abdo *et al.*, Astrophys. J. **658**, L33 (2007).
[10] M. Amenomori *et al.*, in *Turbulence and Nonlinear Processes in Astrophysical Plasmas*, AIP Conf. Proc. No. 932 (AIP, New York, 2007), p. 283.
[11] J. L. Han, R. N. Manchester, A. G. Lyne, G. J. Qiao, and W. van Straten, Astrophys. J. **642**, 868 (2006).
[12] L. Drury and F. Aharonian, Astropart. Phys. **29**, 420 (2008).
[13] M. Witte, M. Banaszkiewicz, H. Rosenbauer, and D. McMullin, Adv. Space Res. **34**, 61 (2004).